Supplementary File to "Multi-channel Weighted Nuclear Norm Minimization for Real Color Image Denoising"

Anonymous ICCV submission

Paper ID 572

In this supplementary file, we provide:

1. The proof of the Theorem 1 in the main paper.
2. More denoising results on the 24 high quality images from the Kodak PhotoCD dataset.
3. More visual comparisons of denoised images by different methods on the real noisy images of the dataset [1].
4. More visual comparisons of denoised images by different methods on the real noisy images of the dataset [2].

1. Proof of Theorem 1.

Theorem 1. *Assume that the weights in $\boldsymbol{w}$ are in a non-descending order, the sequence $\{\mathbf{X}_k\}$, $\{\mathbf{Z}_k\}$, and $\{\mathbf{A}_k\}$ generated in Algorithm 1 satisfy:*

$$(a) \lim_{k\rightarrow\infty} \|\mathbf{X}_{k+1} - \mathbf{Z}_{k+1}\|_F = 0; \quad (b) \lim_{k\rightarrow\infty} \|\mathbf{X}_{k+1} - \mathbf{X}_k\|_F = 0; \quad (c) \lim_{k\rightarrow\infty} \|\mathbf{Z}_{k+1} - \mathbf{Z}_k\|_F = 0. \tag{1}$$

Proof. 1. Firstly, we prove that the sequence $\{\mathbf{A}_k\}$ generated by Algorithm 1 is upper bounded. Let $\mathbf{X}_{k+1} + \rho_k^{-1}\mathbf{A}_k = \mathbf{U}_k\boldsymbol{\Sigma}_k\mathbf{V}_k^\top$ be its singular value decomposition (SVD) [3] in the $(k+1)$-th iteration. According to Corollary 1 of [4], we can have the SVD of $\mathbf{Z}_{k+1}$ as $\mathbf{Z}_{k+1} = \mathbf{U}_k\hat{\boldsymbol{\Sigma}}_k\mathbf{V}_k^\top = \mathbf{U}_k\mathcal{S}_{\frac{\boldsymbol{w}}{\rho_k}}(\boldsymbol{\Sigma}_k)\mathbf{V}_k^\top$. Then we have

$$\begin{aligned}
\|\mathbf{A}_{k+1}\|_F &= \|\mathbf{A}_k + \rho_k(\mathbf{X}_{k+1} - \mathbf{Z}_{k+1})\|_F = \rho_k\|\rho_k^{-1}\mathbf{A}_k + \mathbf{X}_{k+1} - \mathbf{Z}_{k+1}\|_F && (2)\\
&= \rho_k\|\mathbf{U}_k\boldsymbol{\Sigma}_k\mathbf{V}_k^\top - \mathbf{U}_k\mathcal{S}_{\frac{\boldsymbol{w}}{\rho_k}}(\boldsymbol{\Sigma}_k)\mathbf{V}_k^\top\|_F = \rho_k\|\boldsymbol{\Sigma}_k - \mathcal{S}_{\frac{\boldsymbol{w}}{\rho_k}}(\boldsymbol{\Sigma}_k)\|_F && (3)\\
&= \rho_k\sqrt{\sum_i(\boldsymbol{\Sigma}_k^{ii} - \mathcal{S}_{\frac{w_i}{\rho_k}}(\boldsymbol{\Sigma}_k^{ii}))^2} \le \rho_k\sqrt{\sum_i(\frac{w_i}{\rho_k})^2} = \sqrt{\sum_i w_i^2}. && (4)
\end{aligned}$$

The inequality in the second last step can be proved as follows: given the diagonal matrix $\boldsymbol{\Sigma}_k$, we define $\boldsymbol{\Sigma}_k^{ii}$ as the i-th element of $\boldsymbol{\Sigma}_k^{ii}$. If $\boldsymbol{\Sigma}_k^{ii} \ge \frac{w_i}{\rho_k}$, we have $\mathcal{S}_{\frac{w_i}{\rho_k}}(\boldsymbol{\Sigma}_k^{ii}) = \boldsymbol{\Sigma}_k^{ii} - \frac{w_i}{\rho_k} \ge 0$. If $\boldsymbol{\Sigma}_k^{ii} < \frac{w_i}{\rho_k}$, we have $\mathcal{S}_{\frac{w_i}{\rho_k}}(\boldsymbol{\Sigma}_k^{ii}) = 0 < \boldsymbol{\Sigma}_k^{ii} + \frac{w_i}{\rho_k}$. After all, we have $|\boldsymbol{\Sigma}_k^{ii} - \mathcal{S}_{\frac{w_i}{\rho_k}}(\boldsymbol{\Sigma}_k^{ii})| \le \frac{w_i}{\rho_k}$ and hence the inequality holds true. Hence, the sequence $\{\mathbf{A}_k\}$ is upper bounded.

2. Secondly, we prove that the sequence of Lagrangian function $\{\mathcal{L}(\mathbf{X}_{k+1}, \mathbf{Z}_{k+1}, \mathbf{A}_k, \rho_k)\}$ is also upper bounded. Since the global optimal solution of $\mathbf{X}$ and $\mathbf{Z}$ in corresponding subproblems, we always have $\mathcal{L}(\mathbf{X}_{k+1}, \mathbf{Z}_{k+1}, \mathbf{A}_k, \rho_k) \le \mathcal{L}(\mathbf{X}_k, \mathbf{Z}_k, \mathbf{A}_k, \rho_k)$. Based on the updating rule that $\mathbf{A}_{k+1} = \mathbf{A}_k + \rho_k(\mathbf{X}_{k+1} - \mathbf{Z}_{k+1})$, we have $\mathcal{L}(\mathbf{X}_{k+1}, \mathbf{Z}_{k+1}, \mathbf{A}_{k+1}, \rho_{k+1}) = \mathcal{L}(\mathbf{X}_{k+1}, \mathbf{Z}_{k+1}, \mathbf{A}_k, \rho_k) + \langle\mathbf{A}_{k+1} - \mathbf{A}_k, \mathbf{X}_{k+1} - \mathbf{Z}_{k+1}\rangle + \frac{\rho_{k+1}-\rho_k}{2}\|\mathbf{X}_{k+1} - \mathbf{Z}_{k+1}\|_F^2 = \mathcal{L}(\mathbf{X}_{k+1}, \mathbf{Z}_{k+1}, \mathbf{A}_k, \rho_k) + \frac{\rho_{k+1}+\rho_k}{2\rho_k^2}\|\mathbf{A}_{k+1} - \mathbf{A}_k\|_F^2$. Since the sequence $\{\|\mathbf{A}_k\}$ is upper bounded, the sequence $\{\|\mathbf{A}_{k+1} - \mathbf{A}_k\|_F\}$ is also upper bounded. Denote by a the upper bound of $\{\|\mathbf{A}_{k+1} - \mathbf{A}_k\|_F\}$, we have $\mathcal{L}(\mathbf{X}_{k+1}, \mathbf{Z}_{k+1}, \mathbf{A}_{k+1}, \rho_{k+1}) \le \mathcal{L}(\mathbf{X}_1, \mathbf{Z}_1, \mathbf{A}_0, \rho_0) + a\sum_{k=0}^{\infty}\frac{\rho_{k+1}+\rho_k}{2\rho_k^2} = \mathcal{L}(\mathbf{X}_1, \mathbf{Z}_1, \mathbf{A}_0, \rho_0) + a\sum_{k=0}^{\infty}\frac{\mu+1}{2\mu^k\rho_0} \le \mathcal{L}(\mathbf{X}_1, \mathbf{Z}_1, \mathbf{A}_0, \rho_0) + \frac{a}{\rho_0}\sum_{k=0}^{\infty}\frac{1}{\mu^{k-1}}$. The last inequality holds since $\mu + 1 < 2\mu$. Since $\sum_{k=0}^{\infty}\frac{1}{\mu^{k-1}} < \infty$, the sequence of Lagrangian function $\mathcal{L}(\mathbf{X}_{k+1}, \mathbf{Z}_{k+1}, \mathbf{A}_{k+1}, \rho_{k+1})$ is upper bound.

3. Thirdly, we prove that the sequences of $\{\mathbf{X}_k\}$ and $\{\mathbf{Z}_k\}$ are upper bounded. Since $\|\mathbf{W}(\mathbf{Y} - \mathbf{X})\|_F^2 + \|\mathbf{Z}\|_{\boldsymbol{w},*} = \mathcal{L}(\mathbf{X}_k, \mathbf{Z}_k, \mathbf{A}_{k-1}, \rho_{k-1}) - \langle\mathbf{A}_k, \mathbf{X}_k - \mathbf{Z}_k\rangle - \frac{\rho_k}{2}\|\mathbf{X}_k - \mathbf{Z}_k\|_F^2 = \mathcal{L}(\mathbf{X}_k, \mathbf{Z}_k, \mathbf{A}_{k-1}, \rho_{k-1}) + \frac{1}{2\rho_k}(\|\mathbf{A}_{k-1}\|_F^2 - \|\mathbf{A}_k\|_F^2)$. Thus $\{\mathbf{W}(\mathbf{Y} - \mathbf{X}_k)\}$ and $\{\mathbf{Z}_k\}$ are upper bounded, and hence the sequence $\{\mathbf{X}_k\}$ is bounded by the Cauchy-Schwarz inequality

Table 1. PSNR(dB) results of different denoising methods on 24 natural images.

	$\sigma_r = 5, \sigma_g = 30, \sigma_b = 15$								
Image#	**CBM3D**	**MLP**	**TNRD**	**NI**	**NC**	**WNNM-1**	**WNNM-2**	**WNNM-3**	**MC-WNNM**
1	27.25	28.06	28.62	25.00	29.55				
2	29.70	31.30	32.70	27.80	29.69				
3	30.34	31.98	34.07	28.02	31.93				
4	29.47	31.10	32.56	27.70	32.56				
5	27.31	28.59	29.35	26.14	30.00				
6	28.20	29.10	29.90	26.15	28.81				
7	29.73	31.60	33.46	27.22	31.63				
8	27.47	28.16	28.91	25.34	30.16				
9	30.07	31.63	33.55	27.86	31.54				
10	29.96	31.37	33.20	27.74	33.44				
11	28.73	29.85	30.87	26.98	30.16				
12	30.20	31.50	33.31	27.97	31.69				
13	26.18	26.69	26.98	25.14	27.97				
14	27.86	29.07	29.87	26.67	29.21				
15	29.91	31.58	33.13	28.04	31.17				
16	29.29	30.35	31.54	27.46	32.18				
17	29.50	31.09	32.52	27.81	32.80				
18	27.72	28.74	29.36	26.57	28.63				
19	28.98	30.18	31.35	27.25	29.79				
20	30.63	31.78	33.27	27.89	29.52				
21	28.50	29.58	30.54	26.86	31.71				
22	28.61	29.78	30.82	27.19	30.50				
23	30.60	32.66	35.06	28.17	32.82				
24	27.97	28.81	29.61	26.01	30.75				
Average	28.92	30.19	31.44	27.04	30.76	31.89			

and triangle inequality. We can obtain that $\lim_{k\rightarrow\infty}\|\mathbf{X}_{k+1}-\mathbf{Z}_{k+1}\|_F = \lim_{k\rightarrow\infty}\rho_k^{-1}\|\mathbf{A}_{k+1}-\mathbf{A}_k\|_F = 0$ and the equation (a) is proved.

4. Then we can prove that $\lim_{k\rightarrow\infty}\|\mathbf{X}_{k+1}-\mathbf{X}_k\|_F = \lim_{k\rightarrow\infty}\|(\mathbf{W}^\top\mathbf{W}+\frac{\rho_k}{2}\mathbf{I})^{-1}(\mathbf{W}^\top\mathbf{W}\mathbf{Y}-\mathbf{W}^\top\mathbf{W}\mathbf{Z}_k-\frac{1}{2}\mathbf{A}_k)-\rho_k^{-1}(\mathbf{A}_k-\mathbf{A}_{k-1})\|_F \leq \lim_{k\rightarrow\infty}\|(\mathbf{W}^\top\mathbf{W}+\frac{\rho_k}{2}\mathbf{I})^{-1}(\mathbf{W}^\top\mathbf{W}\mathbf{Y}-\mathbf{W}^\top\mathbf{W}\mathbf{Z}_k-\frac{1}{2}\mathbf{A}_k)\|_F+\rho_k^{-1}\|\mathbf{A}_k-\mathbf{A}_{k-1}\|_F = 0$ and hence (b) is proved.

5. Finally, (c) can be proved by checking that $\lim_{k\rightarrow\infty}\|\mathbf{Z}_{k+1}-\mathbf{Z}_k\|_F = \lim_{k\rightarrow\infty}\|\mathbf{X}_k+\rho_k^{-1}\mathbf{A}_{k-1}-\mathbf{Z}_k+\mathbf{X}_{k+1}-\mathbf{X}_k+\rho_k^{-1}\mathbf{A}_{k-1}+\rho_k^{-1}\mathbf{A}_k-\rho_k^{-1}\mathbf{A}_{k+1}\|_F \leq \lim_{k\rightarrow\infty}\|\mathbf{\Sigma}_{k-1}-\mathcal{S}_{\boldsymbol{w}/\rho_{k-1}}(\mathbf{\Sigma}_{k-1})\|_F+\|\mathbf{X}_{k+1}-\mathbf{X}_k\|_F+\rho_k^{-1}\|\mathbf{A}_{k-1}+\mathbf{A}_{k+1}-\mathbf{A}_k\|_F = 0$, where $\mathbf{U}_{k-1}\mathbf{\Sigma}_{k-1}\mathbf{V}_{k-1}^\top$ is the SVD of the matrix $\mathbf{X}_k+\rho_{k-1}\mathbf{A}_{k-1}$. □

2. More denoising results on the 24 high quality images from the Kodak PhotoCD dataset

In the main paper, we have given the PSNR results of the competing methods on the 24 high quality images from the Kodak PhotoCD dataset when the noise standard deviations are $\sigma_r = 40, \sigma_g = 20, \sigma_b = 30$. Here we provide more denoising results on this dataset. In Tables **??**-**??**, we give more PSNR results on these images when the noise standard deviations are $\sigma_r = 5, \sigma_g = 30, \sigma_b = 15$ in Table 1 and $\sigma_r = 30, \sigma_g = 10, \sigma_b = 50$ in Table 2, respectively. In Figures 1-**??**, we give the visual comparisons of the denoised images by different methods.

Fig. 1 shows a scene denoised by the compared methods. We can see that the methods of CBM3D and NC would remain some noise on the recovered images. The methods of MLP, TNRD, and "WNNM0", which process separately the channels of color images, would over-smooth the images and generate false colors or artifacts. The method "WNNM1", which process jointly the channels of color images, would not generate false colors, but still over-smooth the image. The "WNNM2", which is the WNNM model solved by ADMM algorithm, would remain some noise on the image. By employing the proposed MC-WNNM model, our method preserves the structures (e.g., textures in windows and grass) better across the R, G, B channels and generate less artifacts than other denoising methods, leading to visually pleasant outputs.

Table 2. PSNR(dB) results of different denoising methods on 24 natural images.

	$\sigma_r = 30, \sigma_g = 10, \sigma_b = 50$								
Image#	**CBM3D**	**MLP**	**TNRD**	**NI**	**NC**	**WNNM-1**	**WNNM-2**	**WNNM-3**	**MC-WNNM**
1	23.38	26.49	26.50	24.82	23.59				
2	25.19	30.94	30.90	26.82	27.79				
3	25.39	32.03	32.09	27.52	27.41				
4	24.96	30.55	30.47	27.34	27.00				
5	23.29	26.65	26.73	25.72	26.67				
6	24.09	27.76	27.70	26.10	26.12				
7	24.89	30.70	30.72	27.17	28.07				
8	23.30	26.12	26.27	25.59	26.11				
9	25.20	31.35	31.31	27.74	28.33				
10	25.13	31.01	31.05	27.60	28.53				
11	24.54	28.79	28.82	26.72	23.52				
12	25.43	31.60	31.60	27.82	29.01				
13	22.50	24.71	24.73	24.96	23.45				
14	23.91	27.69	27.72	26.26	23.08				
15	25.45	31.09	31.05	27.36	28.49				
16	24.89	29.79	29.73	27.35	27.10				
17	25.12	30.26	30.24	27.15	27.54				
18	23.83	27.26	27.26	26.05	26.15				
19	24.63	29.40	29.39	27.06	27.41				
20	26.43	31.16	31.27	26.43	26.92				
21	24.24	28.26	28.27	26.66	27.18				
22	24.51	29.03	29.06	26.83	27.64				
23	25.55	32.87	32.75	27.60	23.75				
24	23.85	27.06	27.13	25.86	27.05				
Average	24.57	29.27	29.28	26.68	26.58				

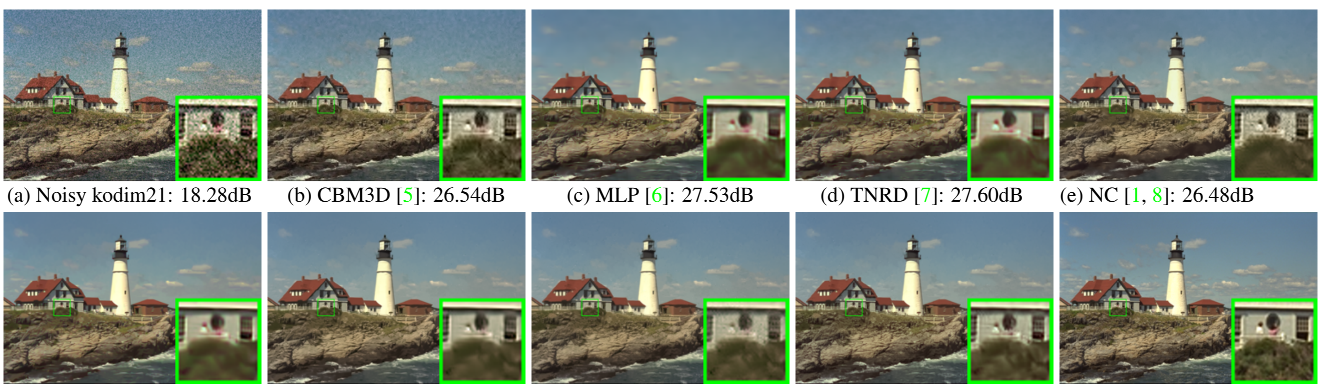

(a) Noisy kodim21: 18.28dB (b) CBM3D [5]: 26.54dB (c) MLP [6]: 27.53dB (d) TNRD [7]: 27.60dB (e) NC [1, 8]: 26.48dB

(f) WNNM0: 27.80dB (g) WNNM1: 27.75dB (h) WNNM2: 27.12dB (i) MC-WNNM: **28.34**dB (j) Clean kodim21

Figure 1. Denoised images of different methods on the image "kodim21" degraded by AWGN with different standard derivations of $\sigma_r = 40, \sigma_g = 20, \sigma_b = 30$ on R, G, B channels, respectively. The images are better to be zoomed in on screen.

3. More visual comparisons of denoised images by different methods on the real noisy images of the dataset [1]

4. More visual comparisons of denoised images by different methods on the real noisy images of the dataset [2]

References

[1] M. Lebrun, M. Colom, and J. M. Morel. The noise clinic: a blind image denoising algorithm. http://www.ipol.im/pub/art/2015/125/. Accessed 01 28, 2015. 1, 3

[2] S. Nam, Y. Hwang, Y. Matsushita, and S. J. Kim. A holistic approach to cross-channel image noise modeling and its application to image denoising. *IEEE Conference on Computer Vision and Pattern Recognition (CVPR)*, pages 1683–1691, 2016. 1, 3

[3] C. Eckart and G. Young. The approximation of one matrix by another of lower rank. *Psychometrika*, 1(3):211–218, 1936. 1

[4] S. Gu, Q. Xie, D. Meng, W. Zuo, X. Feng, and L. Zhang. Weighted nuclear norm minimization and its applications to low level vision. *International Journal of Computer Vision*, pages 1–26, 2016. 1

[5] K. Dabov, A. Foi, V. Katkovnik, and K. Egiazarian. Color image denoising via sparse 3D collaborative filtering with grouping constraint in luminance-chrominance space. *IEEE International Conference on Image Processing (ICIP)*, pages 313–316, 2007. 3

[6] H. C. Burger, C. J. Schuler, and S. Harmeling. Image denoising: Can plain neural networks compete with BM3D? *IEEE Conference on Computer Vision and Pattern Recognition (CVPR)*, pages 2392–2399, 2012. 3

[7] Y. Chen, W. Yu, and T. Pock. On learning optimized reaction diffusion processes for effective image restoration. *IEEE Conference on Computer Vision and Pattern Recognition (CVPR)*, pages 5261–5269, 2015. 3

[8] M. Lebrun, M. Colom, and J.-M. Morel. Multiscale image blind denoising. *IEEE Transactions on Image Processing*, 24(10):3149–3161, 2015. 3